Green's function nonequilibrium molecular dynamics method for solid surfaces and interfaces

Seiji Kajita
Istituto Nanoscienze, CNR-Consiglio Nazionale delle Ricerche, Via Campi 213A, I-41125 Modena, Italy
and Toyota Central R&D Labs., Inc., 41-1, Yokomichi, Nagakute, Aichi 480-1192, Japan
(Received 25 March 2016; revised manuscript received 8 June 2016; published 12 September 2016)

This study presents a comprehensive procedure to calculate the exact dynamic Green's function of a harmonic semi-infinite solid and the time trajectories of the atoms, in the framework of the Green's function molecular dynamics. This Green's function properly describes the energy dissipation caused by excitations of the surface phonons, and the simulated atoms serve as well-defined thermo- and barostats for the nonequilibrium surface and interface systems. Moreover, the use of the exact dynamic Green's function coupled with a fast convolution algorithm significantly improves both the accuracy and the computing speed. The presented method is applied to a diamond (001) surface, and the results demonstrate that the properties of the nonreflecting boundary, the thermal fluctuations, and the energy dissipations involving long-wavelength phonons are correctly reproduced. These distinctive performances potentially allow us to reveal the nonequilibrium phenomena in a wide spectrum of applications such as catalysis, thermal transport, fracture mechanics, mechanochemistry, and tribology.

DOI: 10.1103/PhysRevE.94.033301

I. INTRODUCTION

Pressing demands to reduce energy consumption have heightened the need to predict energy transports and dissipations at solid surfaces and interfaces in multidisciplinary fields [1], which involve solid catalysis [2], thermal transport of nanostructured materials [3,4], dynamic fractures [5,6], mechanochemistry [7], and frictions between sliding solid interfaces [8,9]. Since it is extremely challenging to access the buried nonequilibrium interface through nanoscale experiments [10,11], molecular dynamics (MD) and *ab initio* calculations have been often employed to reveal the atomistic mechanisms [12–16]. These atomistic simulations, however, are prone to provide artificial influences on the results due to the restricted calculable wavelength of the surface phonons. Indeed, several studies have reported that energy-dissipation properties associated with phonons, such as thermal conductivity and friction force, significantly depend on the size of the simulated systems [4,17–20]. Another problem arises from the thermo- and barostats methodologies [21–29]. For instance, a conventional technique of a Nosé-Hoover thermostat based on the *NVT* ensembles in thermal equilibrium is not well defined for nonequilibrium systems [30,31]; in fact, it is known that nonlinear transport properties are influenced by the type of the thermostat used in the MD simulation [24].

Among many potential methods that attempt to overcome the limitations described above [32–38], Green's function methods are of special interest. This approach allows us to focus on a central region by taking into account also the infinite degrees of freedom of the surrounding atoms [39,40]. For surface systems, for example, by considering a semi-infinite solid as a harmonic bath, we can derive the generalized Langevin equation in which all the degrees of freedom of infinitely large number of the solid atoms are projected on the surface atoms in the simulation cell [30,31,41–43]. This formulation enables us to simulate the surface atoms of the semi-infinite solid without explicit calculations of the internal atoms of the solid.

This semi-infinite Green's function approach has been successfully applied to assess static properties of mechanical contacts [44,45], adsorbates [46,47], and electronic structures of surfaces [48–54]. However, difficulties still remain in practical implementations for the dynamical simulation, i.e., Green's function MD (GFMD). The main problems involve (1) the determination of a realistic, accurate, and easily calculable form for the Green's function and (2) the evaluation of the convolution integral, which would become a critical bottleneck for the actual simulations of the time evolution [30,44,55]. To overcome these drawbacks, numerous attempts have been developed by means of the expansion by the continued fraction form [56], the assumptions in the function form composed of Gaussian and stationary vibrations [55,57], the decomposition with eigenfrequencies and eigenvectors of the solid of finite size [31,58,59], the estimation from a long MD run based on the fluctuation dissipation theorem [44,60,61], and the auxiliary dynamic degrees of freedom introduced to the equations of motion [62–65]. The performances of all these methods, however, crucially depend on the arbitrary parameters that must be chosen so as to optimize the accuracy of the approximated Green's functions in their frameworks. Therefore, an *exact* approach with applicable computational loads is needed in order to secure and spread the use of the GFMD simulations.

This study provides a comprehensive recipe of the exact GFMD approach for the harmonic semi-infinite solid. The main idea is to derive the analytic Green's function in the complex space by exploiting the fact that semi-infinite solids are invariant with respect to the addition or the removal of surface layers [52–54]. This exact Green's function allows us to use a fast convolution method combined with the inverse Laplace transformation, and thus the computational costs due to the convolution term are dramatically reduced [66–70]. These improvements render the method applicable also to large systems of higher importance in realistic simulations that were previously considered too demanding. Moreover, schemes to make the GFMD atoms behave as proper thermo- and barostats for solid surfaces and interfaces are also presented.

This paper is organized as follows. Section II describes the theory and the algorithm of the GFMD method. The GFMD method is applied to diamond (001) surfaces in simple nonequilibrium systems of collisions of gas atoms,

thermal fluctuations, and sliding friction. The test conditions and results are reported in Secs. III and IV, respectively. The movies of the simulations are also provided in the Supplemental Material [71]. Conclusions are drawn in Sec. V.

II. THEORY

A. Green's function

Let us consider a unitcell that contains atoms connected to each other and repeats in the surface lateral directions so as to form a solid layer. The periodic boundary conditions are imposed on the boundary of the solid layer. The solid layers, then, are stacked along the surface normal direction, interacting with their nearest-neighbor layers in such a way as to form a semi-infinite solid. Assuming that the intrabonds among the atoms are elastic, the equation of motion for the entire solid is

$$\left(M\frac{d^2}{dt^2}+D^0\right)\mathbf{u}^0(t)=\mathbf{f}^{\mathbf{0}}(t),$$

where $\mathbf{u}^{\mathbf{0}}$, $\mathbf{f}^{\mathbf{0}}$, and M are the atomic displacement vector, external force vector, and the atomic mass matrix, respectively. The dynamical matrix D^0 consists of the elastic force terms for all the atoms in the solid. Note that uppercase, bold, and lowercase letters are employed to indicate matrices, vectors, and scalars, respectively. The above equation can be expressed in a simpler form by mass normalization with a $\mathcal{N}$ matrix defined as $\mathcal{N}^2=M^{-1}$. Transforming the quantities as $D^0=\mathcal{N}^{-1}D\mathcal{N}^{-1}$, $\mathbf{u}^{\mathbf{0}}=\mathcal{N}\mathbf{u}$, and $\mathbf{f}^{\mathbf{0}}=\mathcal{N}^{-1}\mathbf{f}$, we obtain

$$\left(\frac{d^2}{dt^2}+D\right)\mathbf{u}(t)=\mathbf{f}(t). \tag{1}$$

Here we consider a surface lattice vector $\mathbf{r}_{//}$ that consists of the lattice-vector components parallel to the surface. Discrete Fourier transformations between $\mathbf{r}_{//}$ basis and the surface reciprocal vector $\mathbf{k}_{//}$ basis are defined with respect to arbitrary vector $\mathbf{x}$ and matrix X as

$$\mathbf{x}(\mathbf{k}_{//})=\sum_{\mathbf{r}_{//}}\exp(-\mathrm{i}\mathbf{k}_{//}\cdot\mathbf{r}_{//})\mathbf{x}(\mathbf{r}_{//})/\sqrt{n},$$

$$X(\mathbf{k}_{//},\mathbf{k}'_{//})=\sum_{\mathbf{r}_{//},\mathbf{r}'_{//}}\exp(-\mathrm{i}\mathbf{k}_{//}\cdot\mathbf{r}_{//})X(\mathbf{r}_{//},\mathbf{r}'_{//})\times\exp(\mathrm{i}\mathbf{k}'_{//}\cdot\mathbf{r}'_{//})/n,$$

where n is the number of the unit cells contained in a solid layer. In the following, a matrix notation $X(\mathbf{x})$ is used when a matrix is diagonal with respect to the $\mathbf{x}$ base. According to the surface periodicity and Bloch's theorem, Eq. (1) can be diagonalized by moving to the $\mathbf{k}_{//}$ space. In the initial conditions $\mathbf{u}(t=0)=\dot{\mathbf{u}}(t=0)=0$, we can define the Green's function of the semi-infinite solid through the discrete Fourier and the Laplace transformations of Eq. (1) as

$$G(z,\mathbf{k}_{//})=[z^2+D(\mathbf{k}_{//})]^{-1}, \tag{2}$$

where z represents a coordinate point in the complex plane.

The direct solution of Eq. (2) is notoriously difficult, because one must treat the dynamical matrix which contains the infinite degrees of freedom. This difficulty can be circumvented by considering a self-evident property, the semi-infinite periodicity (SIP), which states that the dynamical properties depend on neither addition nor removal of a finite number of unit layers [52–54].

In order to lay the SIP on the present system, we treat each solid layer individually by labeling from the top to the bottom as $\xi=1,2,\ldots,\infty$. An external force $\mathbf{f}_1$ is assumed to affect only the top layer ($\xi=1$). The displacement of the top layer, $\mathbf{u}_1$, is given by

$$\mathbf{u}_1(z,\mathbf{k}_{//})=G_{11}(z,\mathbf{k}_{//})\mathbf{f}_1(z,\mathbf{k}_{//}), \tag{3}$$

where $G_{11}=G_{\xi=1,\xi'=1}$. To make the notations simpler, the variables z and $\mathbf{k}_{//}$ will be omitted if not specifically mentioned. In the $\mathbf{r}_{//}$ basis, Eq. (3) becomes

$$\mathbf{u}_1(\mathbf{r}_{//})=\sum_{\mathbf{r}'_{//}}G_{11}(\mathbf{r}_{//},\mathbf{r}'_{//})\mathbf{f}_1(\mathbf{r}'_{//}). \tag{4}$$

Then a new layer labeled by $\xi=0$, which is identical to the others, is piled on top of the layer $\xi=1$ with the same interlayer potential. The dynamical matrix of the new layer, $D_{00}=D_{\xi=0,\xi'=0}$, consists of elastic terms that come from the layer itself and the interaction with the $\xi=1$ layer; namely, it can be decomposed with $D_{00}=L+D'_{00}$, where L is the elastic force matrix within the layer and the matrix D'_{00} is the elastic interlayer-force term with respect to the displacement of the $\xi=0$ layer. The motion equation of the displacement $\mathbf{u_0}$ of the newly added layer is

$$\begin{aligned}z^2\mathbf{u_0}(\mathbf{r}_{//})&=-\sum_{\mathbf{r}'_{//}}L(\mathbf{r}_{//},\mathbf{r}'_{//})\mathbf{u_0}(\mathbf{r}'_{//})\\&\quad-D'_{00}\mathbf{u_0}(\mathbf{r}_{//})-\sum_{\mathbf{r}'_{//}}D_{01}(\mathbf{r}_{//},\mathbf{r}'_{//})\mathbf{u}_1(\mathbf{r}'_{//})+\mathbf{f_0}(\mathbf{r}_{//}),\end{aligned} \tag{5}$$

where $\mathbf{f_0}$ is an external force applied on the layer $\xi=0$. The external force $\mathbf{f}_1$ in Eq. (4), in turn, becomes the counteracting force due to the interlayer interaction with $\mathbf{u_0}$, as

$$\mathbf{u}_1(\mathbf{r}_{//})=\sum_{\mathbf{r}'_{//}}G_{11}(\mathbf{r}_{//},\mathbf{r}'_{//})\times\left[D'_{11}\mathbf{u}_1(\mathbf{r}'_{//})+\sum_{\mathbf{r}'_{//}}D_{10}(\mathbf{r}'_{//},\mathbf{r}'_{//})\mathbf{u_0}(\mathbf{r}'_{//})\right], \tag{6}$$

where $D'_{11}=D_{11}-L$ and D_{10} are the counterforce terms against the D'_{00} and D_{01} terms, respectively. Transformed to the $\mathbf{k}_{//}$ space, the simultaneous Eqs. (5) and (6) yield

$$(z^2+L+\tilde{D}_{00})\mathbf{u_0}=\mathbf{f_0}, \tag{7}$$

where $\tilde{D}_{00}$ is an effective interlayer matrix:

$$\tilde{D}_{00}(G_{11})=D'_{00}+D_{01}(\mathbf{k}_{//})(1-G_{11}\,D'_{11})^{-1}G_{11}\,D_{10}(\mathbf{k}_{//}). \tag{8}$$

Since the displacement $\mathbf{u_0}$ becomes that for the top layer in the semi-infinite solid, the form of Eq. (7) must be identical to that of Eq. (3) to satisfy the SIP. Therefore, a matrix equation

for G_{11} is given by

$$G_{11}(z,\mathbf{k}_{//}) = [z^2 + L(\mathbf{k}_{//}) + \tilde{D}_{00}(G_{11})]^{-1}. \tag{9}$$

Equations (8) and (9) are the key formulas to compute the exact Green's function. The internal force matrices L, D'_{00}, D'_{11}, D_{10}, and D_{01} are extracted from *ab initio* calculations on solid systems [72,73].

Numerical solutions of the Green's functions can be derived by conventional Newton-Raphson algorithms [74], which require the Jacobian matrix. By introducing $\Gamma = G_{11}^{-1}$ in Eqs. (8) and (9), a nonlinear function W can be defined as

$$W(\Gamma^m) = z^2 + L + \tilde{D}_{00}(\Gamma^m) - \Gamma^m, \tag{10}$$

where the superscript m indicates a number of iterative steps of the trial function Γ^m. With a vector expression for the matrix elements $W_{i,j}$, in which the indices i and j label the atoms, the multivariables Newton-Raphson algorithm presents

$$\begin{bmatrix} \Gamma_{11} \\ \Gamma_{12} \\ \vdots \\ \Gamma_{n_a n_a} \end{bmatrix}_{m+1} = \begin{bmatrix} \Gamma_{11} \\ \Gamma_{12} \\ \vdots \\ \Gamma_{n_a n_a} \end{bmatrix}_{m} - \mu \begin{bmatrix} \frac{\partial W_{11}}{\partial \Gamma_{11}} & \frac{\partial W_{11}}{\partial \Gamma_{12}} & \cdots \\ \frac{\partial W_{12}}{\partial \Gamma_{11}} & \frac{\partial W_{12}}{\partial \Gamma_{12}} & \cdots \\ \vdots & \vdots & \cdots \\ \frac{\partial W_{n_a n_a}}{\partial \Gamma_{11}} & \frac{\partial W_{n_a n_a}}{\partial \Gamma_{12}} & \cdots \end{bmatrix}_m^{-1} \begin{bmatrix} W_{11} \\ W_{12} \\ \vdots \\ W_{n_a n_a} \end{bmatrix}_m, \tag{11}$$

where n_a is the number of the atoms in the unit cell and μ is the damping parameter [74]. The element of the Jacobian matrix is calculated by

$$\frac{\partial W}{\partial \Gamma_{ij}} = -D^{01}\left(\Gamma - D'_{11}\right)^{-1} \frac{\partial \Gamma}{\partial \Gamma_{ij}} \left(\Gamma - D'_{11}\right)^{-1} D_{10} - \frac{\partial \Gamma}{\partial \Gamma_{ij}}. \tag{12}$$

Concerning the initial trial function $\Gamma^{m=0}$, a simple and reasonable choice would be a mixture of two opposite limits: one limit is characterized by $\tilde{D}_{00} = D'_{00}$ in which the top layer is connected to the rigid body, while the other is characterized by $\tilde{D}_{00} = 0$ in which the top layer is free from the semi-infinite substrate in the zero limit of the effective interlayer connection. Therefore, a plausible initial trial function is $\Gamma^{m=0} = z^2 + L(\mathbf{k}_{//}) + \lambda D'_{00}$, where $1 \geqslant \lambda \geqslant 0$ is the mixture parameter.

Some limitations of the current scheme of the Green's function should be mentioned here. Since the semi-infinite solid is approximated as a harmonic solid, this approximation may lead to inaccurate dynamics due to the less realistic description of the intrabonds. This problem, however, would be minimized by considering a hybrid system [37,38] composed of a central region, in which chemical reactions or nonlinearity deformations occur, treated by more realistic methods such as *ab initio* MD and the surrounding region described by the GFMD method. Another drawback is that aperiodic systems such as amorphous materials or systems with impurities cannot be treated.

B. Solutions of the Green's function MD atoms

Once the Green's function is obtained, the time evolution of the GFMD atoms can be computed as

$$\mathbf{v}(t,\mathbf{k}_{//}) = \int_0^t S(t-t',\mathbf{k}_{//})\mathbf{f}(t',\mathbf{k}_{//})\,dt' + \mathbf{v}^{\mathbf{T}}(t,\mathbf{k}_{//}) + \mathbf{v}^{\mathbf{P}}(t,\mathbf{k}_{//}), \tag{13}$$

where $S(t) = \mathcal{N}\frac{d}{dt}G_{11}(t)\mathcal{N}$, and the velocities and the external forces are no longer normalized with respect to the mass. The velocities $\mathbf{v}^{\mathbf{T}}$ and $\mathbf{v}^{\mathbf{P}}$ originate from thermal fluctuations and applied stresses, respectively; they are the general solutions determined by the initial displacements and velocities of the system. The theoretical and numerical details of these solutions are described below.

1. Convolution of the Green's function with external forces

The first term of the right-hand side of Eq. (13) is the velocity dictated by the response of the semi-infinite solid to the external force. A conventional quadrature for the convolution integral requires a simulation time of $O(n_t^2)$ and a memory allocation of $O(n_t)$, where n_t is the total number of the time steps. This demanding computational cost is dramatically reduced by using the fast convolution method combined with the modified-Talbot's inverse Laplace transformation [66–69]. More specifically, the time interval of the convolution is divided by grids, and each convolution component is calculated by the inverse Laplace transformation of $S(z,\mathbf{k}_{//})\mathbf{f}(z,\mathbf{k}_{//})$ along a modified path of integration. The integration path is formulated by bending the Bromwich line in the complex plane so as to optimize the accuracy of the convolution on the discretized time interval. Consequently, this algorithm allows us to compute the convolution precisely by requiring only a simulation time of $O[n_t \log(n_t)]$ and a memory allocation of $O[\log(n_t)]$.

Although several choices are available for the path of the integration [70], an essence of all the procedures is to modify the path so that it embraces the singularity points of $S(\mathrm{i}\omega,\mathbf{k}_{//})$. Prior to the use of the fast convolution methods, thus, the position of the singularities must be identified. An efficient way to locate the singularities is to focus on $\mathrm{Im}\,G_{11}(\mathrm{i}\omega,\mathbf{k}_{//})$, which is associated with the surface density of states [75]. As the infinite degrees of freedom in the solid are projected on the surface atoms, the surface density of states forms a continuous function of the frequency ω [18,19]. The supremum and infimum frequencies in the range of the density of states, in fact, can be located in the singularity points, according to the context of Van Hove singularities [76]. As a result, the singularity points are easily found by searching the frequency range of the $\mathrm{Im}\,G_{11}(\mathrm{i}\omega,\mathbf{k}_{//})$. Because of the divergent property at the singularities, the transition of $\Gamma(\mathrm{i}\omega,\mathbf{k}_{//}) = G_{11}^{-1}$ can be detected more stably in actual simulations.

To integrate numerically along the proper path, note that once $\Gamma(z_i)$ is obtained at a certain discretized point z_i, the initial trial function for the next $\Gamma(z_{i+1})$ should be chosen recursively as $\Gamma^{m=0}(z_{i+1}) = \Gamma(z_i)$. Since the Green's function has the polyvalence property, this procedure is useful to keep the integration path in the one Riemann surface corresponding to the correct inverse Laplace transformation.

2. Temperature

The thermal fluctuation $\mathbf{v^T}$ is caused by the random forces arising from vibrations of the semi-infinite solid placed at a temperature T. From the context of the equation of motion, the velocity $\mathbf{v^T}$ is a linear combination of the general solutions for initial displacements and velocities of the entire solid, which serves as a harmonic bath [39]. Through the fluctuation-dissipation theorem [40], a simple relation between $\mathbf{v^T}$ and the Green's function can be written as

$$\left\langle v^T_{i,j}(t,\mathbf{k}_{//})\, v^T_{i',j'}(t=0,\mathbf{k}_{//})\right\rangle = k_B T\, S_{i,i',j,j'}(t,\mathbf{k}_{//}), \quad (14)$$

where $v^T_{i,j}$ is the velocity of the ith atom in j direction, and $\langle\rangle$ is the ensemble average operator. An established algorithm based on the Fourier series expansion combined with the Gaussian process [77] readily produces $\mathbf{v^T}$ that satisfy both the stochastic movements and the constraint described in Eq. (14) for an arbitrary form of the Green's function.

3. Stress

The barostat scheme in GFMD simulations should be designed in such a way that it reproduces the pressure exerted on a thin layer of liquid or solid confined between two parallel walls of the semi-infinite solids. Suppose that constant and uniform external forces, $\mathbf{f}(t,\mathbf{k}_{//}) = -\mathbf{f_c}\delta_{\mathbf{k}_{//},0}$, are applied on the top layer of the solid at temperature of 0 K. At first, the solid gets distorted, but the distortion process eventually stops ($\mathbf{v}=0$) when the elastic force is balanced with the external force. According to Eq. (13), the general solution with the given initial conditions can be written as

$$\mathbf{v_P}(t,\mathbf{k}_{//}) = \delta_{\mathbf{k}_{//},0}\mathbf{f_c}\int_0^t S(t',\mathbf{k}_{//})\, dt'. \quad (15)$$

This expression can be understood intuitively as follows: once the applied external force is removed, the distorted solid starts rebounding elastically, exerting a pressure as large as that of the applied force. If we assume that the time interval t is much longer than the decay time of $S(t,\mathbf{k}_{//}=0)$, Eq. (15) can be simplified as

$$\mathbf{v_P}(\mathbf{k}_{//}) = \delta_{\mathbf{k}_{//},0}\, \bar{S}\, \mathbf{f_c}, \quad (16)$$

where $\bar{S} = S(z=0,\mathbf{k}_{//}=0)$. Since the coefficients of $\bar{S}$ are calculated from Eq. (9), the magnitude and directions of the applied stresses are controlled by the parameter $\mathbf{f_c}$. Equation (16) holds the same form of a barostat introduced by Butler and Harrowell [28,29], in which the velocity of the pressed wall is proportional to the applied force. Unlike the previously proposed barostats, the present scheme does not have any arbitrary parameters.

C. Energy dissipation

As the last argument of this section, an important relation between the Green's functions and the internal energies is presented. The internal energy relates to the energy dissipation which is a fundamental observable in nonequilibrium phenomena. The change of the internal energy of surface atoms over the time interval Δt is defined by

$$\frac{\Delta U}{\Delta t} = \frac{1}{\Delta t}\sum_{\mathbf{r}_{//}}\int_t^{t+\Delta t} \mathbf{f}(t,\mathbf{r}_{//})\cdot\mathbf{v}(t,\mathbf{r}_{//})\, dt. \quad (17)$$

Suppose that a semi-infinite solid has achieved a stationary state under external forces. This system is observed for Δt that is long enough with respect to the atomic-time scale: i.e., the decay time of the Green's function. The external forces can be expanded by a Fourier series of $\mathbf{f}(t) = \sum_n \exp(\mathrm{i}\omega_n t)\,\mathbf{f}(\omega_n)$, where n is the integer that goes from $-\infty$ to ∞, and $\omega_n = 2n\pi/\Delta t$. By inserting Eq. (13) into Eq. (17), the energy change is decomposed into the surface-phonon modes ω_n and $\mathbf{k}_{//}$ as

$$\frac{\Delta U}{\Delta t} = 2\sum_{\mathbf{k}_{//}}\sum_{n=1}^{\infty}\mathbf{f}^*(\omega_n,\mathbf{k}_{//})\cdot \mathrm{Re}\, S(\mathrm{i}\omega_n,\mathbf{k}_{//})\,\mathbf{f}(\omega_n,\mathbf{k}_{//}) + \bar{\mathbf{f}}\cdot\bar{S}\,(\bar{\mathbf{f}}+\mathbf{f_c}), \quad (18)$$

where $\bar{\mathbf{f}} = \mathbf{f}(\omega_n=0,\mathbf{k}_{//}=0)$. In the derivation of Eq. (18), the terms related to the thermal fluctuations were canceled out due to the randomness. Furthermore, a relation $S(\mathrm{i}\omega_n = 0,\mathbf{k}_{//}) = \delta_{\mathbf{k}_{//},0}\bar{S}$ was used, because the static external force $\mathbf{f}(\omega_n=0,\mathbf{k}_{//}\neq 0)$ produces no velocities of the surface atoms after achievement of the force balance between the $\mathbf{f}(\omega_n = 0,\mathbf{k}_{//}\neq 0)$ and the corresponding elastic forces in the solid.

Equation (18) can be used to identify pivotal surface modes in nonequilibrium phenomena [18,19,78]. As an example, here we consider a friction system which is composed of two identical semi-infinite solids. The two solids are first positioned so as to face each other with their surfaces being in contact. Then they slide relative to each other. This system holds the reflectional symmetry against the interfacial plane. The total internal energy of the sliding system is expressed as $\Delta U_1 + \Delta U_2$, where the subscript indicates each solid. Since the two solids are identical, the scalar quantities ΔU_1 and ΔU_2 are the same values. Moreover, taking into account the law of the conservation of energy for the total system, $\Delta U_1 + \Delta U_2 = 0$; and thus ΔU_1 must be zero. Therefore, Eq. (18) leads to

$$-\bar{\mathbf{f}}\cdot\bar{S}\,(\mathbf{f_c}+\bar{\mathbf{f}}) = 2\sum_{\mathbf{k}_{//}}\sum_{n=1}^{\infty}\mathbf{f}^*(\omega_n,\mathbf{k}_{//})\cdot\mathrm{Re}\, S(\mathrm{i}\omega_n,\mathbf{k}_{//})\,\mathbf{f}(\omega_n,\mathbf{k}_{//}). \quad (19)$$

As discussed in Sec. II B 3, the quantity $\bar{S}\ (\mathbf{f_c}+\bar{\mathbf{f}})$ is equal to the mean velocity of the slab driven by the constant force $\mathbf{f_c}+\bar{\mathbf{f}}$. Because of the balance between the mean forces in the surface normal direction, only the sliding-direction term contributes to the mean velocity, and its magnitude is half of the relative sliding velocity $\bar{\mathbf{V}}$. Using this fact and considering the direction of the sliding velocity opposite to the mean friction force $\bar{\mathbf{f}}$ in Eq. (19), the energy dissipation rate $j_e^{\mathrm{total}} = -\bar{\mathbf{f}}\cdot\bar{\mathbf{V}}$ can be expressed by

$$j_e^{\mathrm{total}} = \sum_{\mathbf{k}_{//}}\sum_{n=1}^{\infty} j_e(\omega_n,\mathbf{k}_{//}),$$
$$j_e(\omega_n,\mathbf{k}_{//}) = 2\mathbf{f}^*(\omega_n,\mathbf{k}_{//})\cdot\mathrm{Re}\, S(\mathrm{i}\omega_n,\mathbf{k}_{//})\,\mathbf{f}(\omega_n,\mathbf{k}_{//}). \quad (20)$$

It is noteworthy to mention that the proportionality coefficient relating the energy dissipation to the the power spectra of the external force is the real part of the Green's function S. The above formula provides a scheme to decompose the energy dissipation with the surface phonon modes to determine essential phonon modes, as will be demonstrated in Sec. IV C.

III. COMPUTATIONAL DETAILS

In order to test the presented GFMD method, a diamond (001) surface is modeled by a (1×1) in-plane sized layer containing four carbon atoms. The periodic boundary conditions are imposed in the surface lateral directions. The internal force matrices of L, D'_{00}, D'_{11}, D_{10}, and D_{01} are obtained by static *ab initio* calculations of the diamond bulk based on density functional theory (DFT) and the DFT linear-response approach to phonon calculations. [72] The pseudopotential and plane-waves computer codes included in the QUANTUM ESPRESSO package are used [73]. The Perdew, Burke, and Ernzerhof generalized gradient approximation is used for the exchange-correlation functional [79]. The electronic wave functions are expanded on a plane-waves basis set with a cutoff energy of 25 Ry, and the ionic species are described by ultra-soft pseudopotentials [80]. The internal force matrices are approximated so that they contain the elements related only to the nearest-neighbor interactions, and the off-diagonal elements of the directional indices are eliminated for the sake of the numerical simplicity. The Green's function is derived from Eqs. (8) and (9) through the damped Newton algorithm.

The diamond layer is attached to the GFMD atoms with the interlayer interactions. The fast convolution method combined with modified-Talbot's inverse Laplace transformation is used to calculate the convolution term. To simulate the time evolution of the GFMD atom, schemes of common MD algorithms can be exploited by reduced external forces defined as

$$\tilde{\mathbf{f}}(t,\mathbf{k}_{//}) = M \int_0^t A(t-t',\mathbf{k}_{//})\mathbf{f}(t',\mathbf{k}_{//})\,dt', \qquad (21)$$

where $A(t) = \frac{d}{dt}S(t)$. The velocity Verlet algorithm is applied to compute the time evolutions with a time step of 0.96 fs.

To evaluate the GFMD method, conventional MD simulations attached to the Nosé-Hoover thermostat are also performed for comparison. In this thermostat, the velocity of the center of mass of the slab each atom belongs to is subtracted from the atomic velocities that enter the thermostat equations. This modification is made to prevent the thermostat from directly being affected by the sliding motion [15,16]. The oscillation frequency of the Nosé-Hoover thermostat is set at 20 THz, which is within a common range for the carbon systems [15,16]. Constant stresses are directly applied on the outer layer of the surface atoms in the sliding slabs [29].

IV. RESULTS AND DISCUSSIONS

A. Collisions of incident atoms

A neon atom is positioned at a distance of 10 bohr above the surface atom of the diamond (001) at temperature of 0 K. Then, it is injected perpendicularly to the diamond surface at 10000 m/s and collides with the surface atoms. The diamond surface is modeled by a carbon layer connected to the GFMD atoms, as illustrated in Fig. 1(a). The interaction between the neon and surface carbons is described by the Lennard-Jones potential

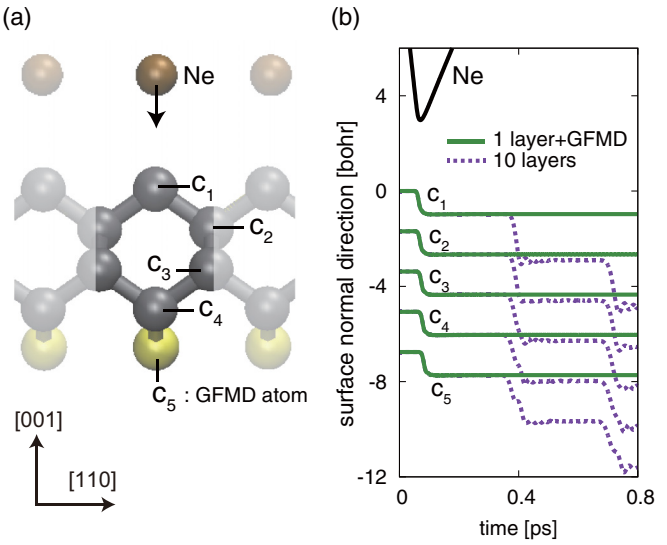

FIG. 1. (a) The collision system attached to the GFMD atom and (b) the atomic displacements along the surface normal direction [001]. The simulation movie is available as Supplemental Material [71].

$$\phi(r) = 4\epsilon\{(\bar{\sigma}/r)^{12} - (\bar{\sigma}/r)^{6}\}, \qquad (22)$$

with $\epsilon = 0.5 \times 10^{-21}$J and the interatomic distance $\bar{\sigma} = 5.08$ bohr [81].

Figure 1(b) shows that the collision of the neon atom causes a downward displacement of the surface carbons, and subsequently the displacement propagates into the inner GFMD atoms. After the first impact, the carbon atoms exhibit no significant movement over time and remain at the shifted positions; namely, the shock wave is eliminated by the GFMD atoms as if the wave keeps traveling in the semi-infinite solid. This nonreflecting effect can be recognized by a direct comparison with a diamond slab of the 10 layers with neither thermostats nor damping terms in the equation of motion. In this case, the displacements reoccur at around 0.4 and 0.7 ps after the collision, as the shock wave is reflected back and forth between the two ends.

B. Thermal fluctuations

In order to gain an insight into thermal fluctuations of the semi-infinite solid system, two different cases are considered: a one-layer diamond slab attached to the GFMD atoms placed at 300 K without external forces and a one-layer slab in the Nosé-Hoover thermostat under the same conditions. The thermal fluctuations of the two systems are simulated and compared to each other.

Figure 2(a) displays the variations of the temperatures in time. Both profiles indicate the mean temperatures $\langle T \rangle$ of 300 K, as initially set. It is difficult to distinguish the two cases by simply observing their variations in time. However, a fundamental difference can be revealed by evaluating the temperature fluctuations. According to statistical mechanics,

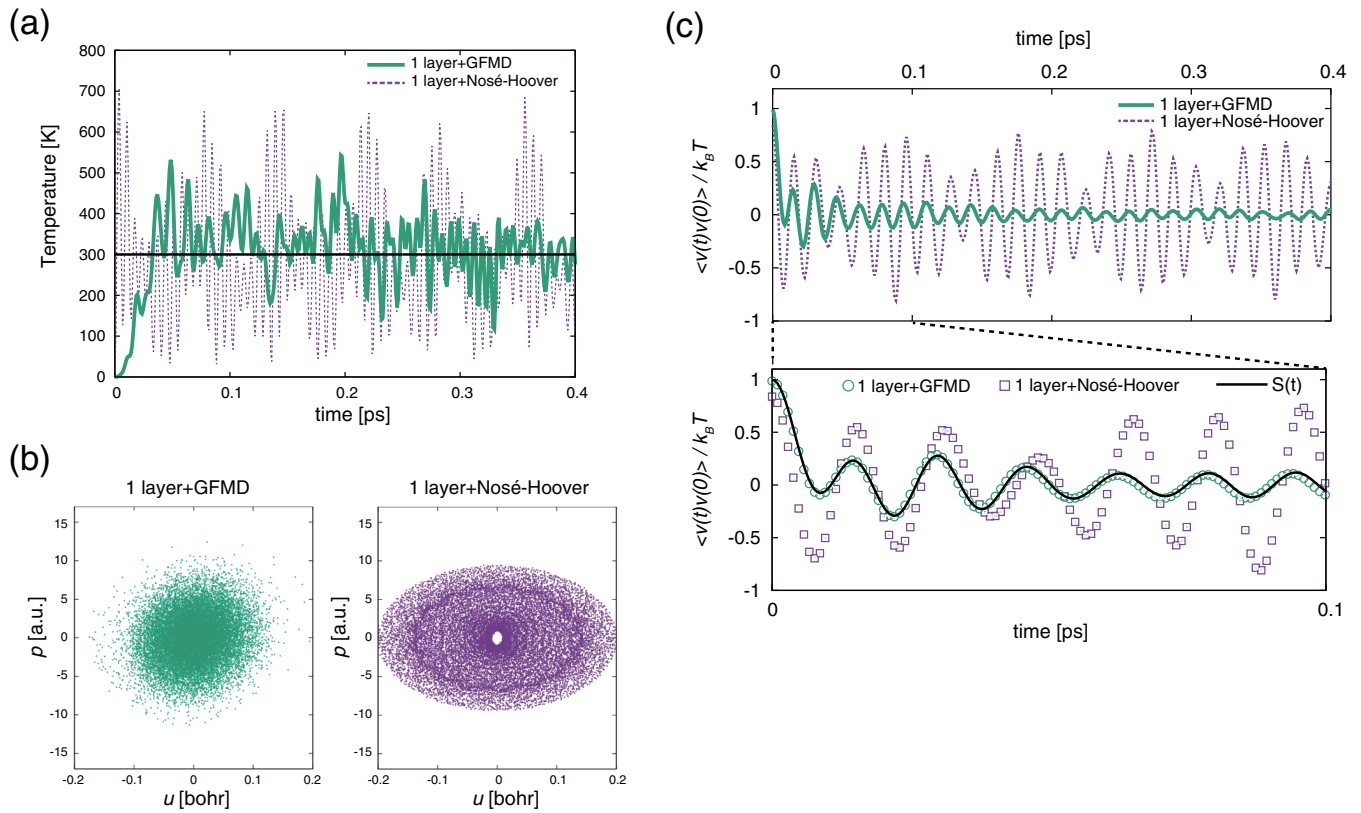

FIG. 2. (a) Time variations of temperatures converted from the total kinetic energies of the diamond slabs and (b) trajectories of the surface atoms in the phase space in the [110] direction. (c) Correlation functions of the thermal velocities in the [110] direction, that are obtained from the ensemble average of 20 trajectories of the surface carbon atoms. The simulation movie is available as Supplemental Material [71].

the temperature fluctuation δT^2 should depend on number of the simulated atoms that are taken into account in the evaluation of the temperature, as

$$\delta T^2 = \langle T^2 \rangle - \langle T \rangle^2 = \frac{2}{3n_a} \langle T \rangle^2, \tag{23}$$

where n_a indicates the number of the simulated atoms. As reported in Table I, the temperature fluctuation of the GFMD system is in good agreement with the theoretical value, while the MD method with the Nose-Hoover thermostat results in the larger fluctuation.

Another essential difference arises from the trajectories of the surface atoms in the phase space as shown in Fig. 2(b). The trajectory in the GFMD system is distributed randomly, being centered at the origin of the phase space. This randomness is consistent with the ergodicity condition which is required for a well-defined heat bath [25]. On the other hand, the trajectory in the system in the Nosé-Hoover thermostat forms a cyclic pattern, which obviously violates the ergodicity. Indeed, it is well known that the extended-variable methodologies including Nosé-Hoover thermostat are unable to produce random trajectories in the solid systems composed of a few atoms, though refined algorithms such as the Nosé-Hoover chain would be able to recover the nonergodic behavior [26,27].

Last, in order to verify the fluctuation-dissipation theorem presented in Eq. (14), the correlation functions of the thermal velocities are evaluated as shown in Fig. 2(c). The correlation function in the GFMD method decays with the time, while that of the system in the Nosé-Hoover thermostat behaves as a steady oscillation. The correlation in the former case, in fact, can be well fitted by the Green's function $S(t)$ of the surface atoms in accordance with the fluctuation-dissipation theorem. Therefore, given the consistencies with the temperature fluctuation, the ergodicity, and the fluctuation-dissipation theorem, the GFMD method functions as a well-defined thermostat for nonequilibrium solid surface and interface systems.

TABLE I. Mean temperatures and temperature fluctuations. The values in the GFMD system and MD system with Nosé-Hoover thermostat are calculated by the simulations of 100 ps long. The theoretical value is obtained using Eq. (23) with $n_a = 4$.

	Theory	GFMD	Nosé-Hoover MD
$\langle T \rangle$ [K]	300	305	291
$\delta T^2/\langle T \rangle^2$	0.167	0.165	0.370

C. Sliding friction

We consider a friction system composed of a pair of diamond slabs which slide relative to each other at 0 K. The two slabs face each other in accordance with the reflectional symmetry against an interfacial middle plane between the two slabs. Each slab is composed of one layer of the diamond, and the GFMD atoms are connected to the opposite sides to the contact interface. This system is compared with a pair of

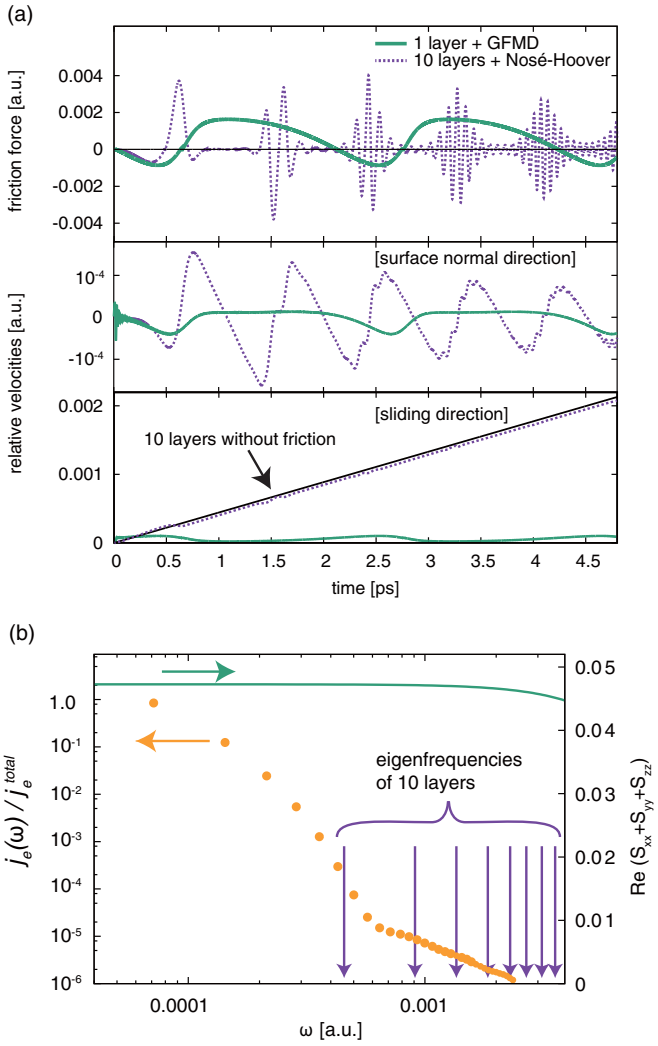

FIG. 3. (a) Time evolutions of the friction forces (upper panel) and relative velocities of the interfacial atoms (middle and lower panels). The friction force is defined by the interaction force which opposes the actual relative sliding motion between two surfaces. (b) Contributions of the phonon modes to the total energy dissipation and real part of the Green's function. To obtain the phonon-modes contributions, the force trajectory ranging from 2.5 ps to 4.6 ps in (a) is used to calculate the power spectrum of the external force in Eq. (20). The simulation movie is available as Supplemental Material [71].

10-layer slabs attached to the Nosé-Hoover thermostat in order to remove friction heat. The dynamical simulations are started from the optimized configuration of the slabs with a contact pressure of 3 GPa. Subsequently, the sliding along the [110] direction is initiated by applying 3 GPa shear stresses on the two slabs opposite to each other. The interfacial atoms are interacting across the slabs via the Lennard-Jones potential shown in Eq. (22) with $\bar{\sigma} = 4.78$ bohr.

Figure 3(a) shows that the friction force of the GFMD system evolves cyclically with a single periodicity. Since the relative velocities of the interfacial atoms share the same periodicity of the force trajectory, this periodicity is related to the movements of the interfacial atoms that climb up and down the potential corrugation of the sliding interface. The force profile of the 10-layer system is considerably different in terms of the two characteristic oscillations. Indeed, we observe the longer periodicity and the shorter periodicity that are attributed to the velocities in the surface normal and sliding directions, respectively. Notice that the sliding speed increases monotonically to reach a large value.

These distinctive differences essentially originate from the difference of time-averaged friction force: i.e., mean friction force. The GFMD system shows a mean friction force of 0.8 GPa. In contrast, the friction force in the ten-layer system oscillates between positive and negative values, which result in a very small net friction. In fact, the tangent of the sliding velocity can be fitted almost perfectly by using the value for a friction-free system in which the interaction force is terminated [black solid line in the lower panel of Fig. 3(a)].

The mechanism behind the difference between the two systems is elucidated by the phonon-modes decomposition of the energy dissipation described in Eq. (20). Since the present system consists of 1×1 unit cells which only contain $\mathbf{k}_{//} = 0$ component, a simplified notation for the decomposed energy dissipation $j_e(\omega) = j_e(\omega_n, \mathbf{k}_{//} = 0)$ is introduced in the following.

Figure 3(b) (circles) shows that $j_e(\omega)$ decreases dramatically as ω increases. The largest contribution, 90% of the total energy dissipation, is found at the lowest frequency called the washboard frequency [82]. Due to the projection of the semi-infinite solid on the GFMD atoms, the surface phonon forms a continuum band of eigenfrequencies [18,19] which dissipates force fluctuations even at zero-limit frequency. In fact, this energy-dissipative band, which is the real part of the Green's function, covers the low-frequency region including the washboard frequency as shown in Fig. 3(b) (solid line). A significant aspect of the washboard frequency, $\omega_1 = 2\pi/\Delta t = \pi\bar{v}/\sigma$ with σ being the surface lattice constant of the unit cell, is that it is associated with the sliding velocity $\bar{v}$, which is of about 120 m/s in the present simulation. This result, therefore, indicates that the surface phonon with the frequency corresponding to the sliding velocity can be excited and drain a considerable amount of the kinetic energy from the sliding interface.

In the ten-layer system, on the other hand, the number of the eigenfrequencies is limited and the discrete frequencies [down arrows in Fig. 3(b)] are distributed in the region higher than the washboard frequency. The key finding is that the finite system cannot excite the slow phonon [17,18] that corresponds to the sliding speed. As a result, the surface repels adiabatically the interaction forces to the countersolid, instead of absorbing the energy from the force fluctuation at the washboard frequency. More specifically, by counting the intersections of $j_e(\omega)$ with the eigenfrequencies of the 10-layer slab, we can estimate that this finite system absorbs less than 0.1% of the energy dissipation that the semi-infinite surface does; this tiny absorption explains the nearly zero friction that we observed.

V. SUMMARY

The present study showed the equation of the exact Green's function in the complex space. Since this equation enables us to employ the fast convolution method combined with the inverse

Laplace transformation, the proposed method provides high accuracy and computing speed in the evaluation of the time evolutions. These improvements make the method applicable also to large systems that are of higher importance in realistic simulations which were previously considered too demanding. The GFMD atoms act as the thermo- and barostats by adding the solutions generated from the interrelations of the Green's function with temperature and stress. Moreover, the GFMD formulation provides an analytical scheme to decompose the energy dissipation with the surface phonon modes to identify the pivotal phonon modes in the nonequilibrium phenomena.

The test simulations demonstrate that the proposed method provides the non-reflecting property of phonons injected from the surface, the thermal fluctuations, and the energy dissipations involving long-wavelength phonons. Since the approach is capable of realizing the non-reflecting boundary, it may provide a crucial step forward in the development of multiscale modeling based on the coupling of atomisticand continuum methodologies [32–36]. Moreover, due to the proper control of temperature and stress, the coupling of *ab initio* MD/GFMD methods [37,38] enables accurate and deep analysis of the reactive nonequilibrium interfaces, leading to a wide range of applications such as catalysis, fracture mechanics, mechanochemistry, and tribochemistry.

ACKNOWLEDGMENTS

The author thanks Dr. M. C. Righi and Prof. M. Ferrario at the University of Modena and Reggio Emilia for fruitful discussions and valuable comments.

[1] E. Pop, Nano Res. **3**, 147 (2010).
[2] B. Gumhalter and T. Matsushima, Surf. Sci. **561**, 183 (2004).
[3] R. J. Stevens, L. V. Zhigilei, and P. M. Norris, Int. J. Heat Mass Transf. **50**, 3977 (2007).
[4] C. Melis, R. Dettori, S. Vandermeulen, and L. Colomboa, Eur. Phys. J. B **87**, 96 (2014).
[5] E. Sharon, S. P. Gross, and J. Fineberg, Phys. Rev. Lett. **76**, 2117 (1996).
[6] D. Holland and M. Marder, Phys. Rev. Lett. **80**, 746 (1998).
[7] S. L. James *et al.*, Chem. Soc. Rev. **41**, 413 (2012).
[8] R. J. Cannara, M. J. Brukman, K. Cimatu, A. V. Sumant, S. Baldelli, and R. W. Carpick, Science **318**, 780 (2007).
[9] K. Saitoh, K. Hayashi, Y. Shibayama, and K. Shirahama, Phys. Rev. Lett. **105**, 236103 (2010).
[10] S. Kajita, K. Yagi, T. Izumi, J. Koyamach, M. Tohyama, K. Saito, and J. Sugimura, Tribol. Lett. **57**, 6 (2015).
[11] K. Yagi, S. Kajita, T. Izumi, J. Koyamachi, M. Tohyama, K. Saito, and J. Sugimura, Tribol. Lett. **61**, 19 (2016).
[12] H. Hitoshi, S. Sand, S. Hyodo, T. Ohmori, N. Nishino, and A. Suzuki, J. Phys.: Conf. Ser. **89**, 012009 (2007).
[13] K. Hayashi, K. Tezuka, N. Ozawa, T. Shimazaki, K. Adachi, and M. Kubo, J. Phys. Chem. C **115**, 22981 (2011).
[14] S. Kajita and M. C. Righi, Tribol. Lett. **61**, 17 (2016).
[15] G. Zilibotti, S. Corni, and M. C. Righi, Phys. Rev. Lett. **111**, 146101 (2013).
[16] S. Kajita and M. C. Righi, Carbon **103**, 193 (2016).
[17] S. Kajita, H. Washizu, and T. Ohmori, Europhys. Lett. **87**, 66002 (2009).
[18] S. Kajita, H. Washizu, and T. Ohmori, Phys. Rev. B **82**, 115424 (2010).
[19] S. Kajita, H. Washizu, and T. Ohmori, Phys. Rev. B **86**, 075453 (2012).
[20] S. Kajita, M. Tohyama, H. Washizu, T. Ohmori, H. Watanabe, and S. Shikata, Tribol. Online **10**, 156 (2015).
[21] S. Nosé, J. Chem. Phys. **81**, 511 (1894).
[22] S. Nosé, Progr. Theor. Phys. Suppl. **103**, 1 (1991).
[23] W. G. Hoover, Phys. Rev. A **31**, 1695 (1985).
[24] P. J. Daivis, B. A. Dalton, and T. Morishita, Phys. Rev. E **86**, 056707 (2012).
[25] P. H. Hünenberger, Adv. Polym. Sci. **173**, 105 (2005).
[26] G. J. Martyna, M. L. Klein, and M. Tuckerman, J. Chem. Phys. **97**, 15 (1992).
[27] P. K. Patra and B. Bhattacharya, J. Chem. Phys. **142**, 194103 (2015).
[28] S. Butler and P. Harrowell, J. Chem. Phys. **118**, 4115 (2003).
[29] C. Gattinoni, S. Mackowiak, D. M. Heyes, A. C. Branka, and D. Dini, Phys. Rev. E **90**, 043302 (2014).
[30] L. Kantorovich, Phys. Rev. B **78**, 094304 (2008).
[31] L. Kantorovich and N. Rompotis, Phys. Rev. B **78**, 094305 (2008).
[32] W. K. Liu, D. Qian, A. Gonella, S. Li, W. Chen, and S. Chirputkar, Int. J. Numer. Meth. Eng. **83**, 1039 (2010).
[33] W. E and Z. Huang, Phys. Rev. Lett. **87**, 135501 (2001).
[34] X. Li and W. E, Phys. Rev. B **76**, 104107 (2007).
[35] G. Anciaux and J. F. Molinari, Int. J. Numer. Methods Eng. **79**, 1041 (2009).
[36] R. Kobayashi, T. Nakamura, and S. Ogata, Int. J. Numer. Methods Eng. **83**, 249 (2010).
[37] N. Ohba, S. Ogata, T. Kouno, T. Tamura, and R. Kobayashi, Comput. Phys. Commun. **183**, 1664 (2012).
[38] M. Swart, Int. J. Quantum Chem. **91**, 177 (2003).
[39] H. Mori, Prog. Theor. Phys. **33**, 423 (1965).
[40] R. Kubo, Rep. Prog. Phys. **29**, 255 (1966).
[41] R. Zwanzig, J. Chem. Phys. **34**, 1173 (1960).
[42] S. A. Adelman and J. D. Doll, J. Chem. Phys. **61**, 4242 (1974).
[43] S. A. Adelman and J. D. Doll, J. Chem. Phys. **64**, 2375 (1976).
[44] C. Campañá and M. H. Müser, Phys. Rev. B **74**, 075420 (2006).
[45] L. T. Kong, G. Bartels, C. Campañá, C. Denniston, and M. H. Müser, Comput. Phys. Commun. **180**, 1004 (2009).
[46] H. Uemura, Y. Saito, and M. Uwaha, J. Phys. Soc. Jpn. **72**, 2856 (2003).
[47] Y. Saito, H. Uemura, and M. Uwaha, Phys. Rev. B **63**, 045422 (2001).
[48] E. J. Mele and J. D. Joannopoulos, Phys. Rev. B **17**, 1816 (1978)
[49] M. P. L. Sancho, J. M. L. Sancho, and J. Rubio, J. Phys. F **14**, 1205 (1984).
[50] J. Velev and W. Butler, J. Phys. Condens. Matter **16**, R637 (2004).
[51] A. Calzolari, T. Jayasekera, K. W. Kim, and M. B. Nardelli, J. Phys. Condens. Matter **24**, 492204 (2012).
[52] A. Gonis, Phys. Rev. B **34**, 8313 (1986).

[53] X. G. Zhang and A. Gonis, Phys. Rev. Lett. **62**, 1161 (1989).
[54] A. Gonis, X. G. Zhang, J. M. MacLaren, and S. Crampin, Phys. Rev. B **42**, 3798 (1990).
[55] A. E. Depristo, Surf. Sci. **141**, 40 (1984).
[56] M. Ferrario and P. Grigolini, Chem. Phys. Lett. **62**, 100 (1979).
[57] J. C. Tully, J. Chem. Phys. **73**, 1975 (1980).
[58] J. A. Barker and W. A. Steele, Surf. Sci. **74**, 596 (1978).
[59] A. Benassi, A. Vanossi, G. E. Santoro, and E. Tosatti, Phys. Rev. B **82**, 081401(R) (2010).
[60] J. E. Straub, M. Borkovec, and B. J. Berne, J. Phys. Chem. **91**, 4995 (1987).
[61] W. Cai, M. de Koning, V. V. Bulatov, and S. Yip, Phys. Rev. Lett. **85**, 3213 (2000).
[62] L. Stella, C. D. Lorenz, and L. Kantorovich, Phys. Rev. B **89**, 134303 (2014).
[63] H. Ness, L. Stella, C. D. Lorenz, and L. Kantorovich, Phys. Rev. B **91**, 014301 (2015).
[64] M. Ceriotti, G. Bussi, and M. Parrinello, Phys. Rev. Lett. **102**, 020601 (2009).
[65] M. Ceriotti, M. Parrinello, and D. E. Manolopoulos, J. Chem. Phys. **134**, 084104 (2011).
[66] A. Talbot, J. Inst. Math. Appl. **23**, 97 (1979).
[67] C. Lubich and A. Schädle, SIAM J. Sci. Comput. **24**, 161 (2002).
[68] G. Capobianco, D. Conte, I. D. Prete, and E. Russo, BIT Numer. Math. **47**, 259 (2007).
[69] I. D. Prete, Efficient numerical methods for Volterra integral equations of Hammerstein type, Doctoral thesis, Università degli Studi di Napoli Federico II, 2006 (http://www.fedoa.unina.it/731/).
[70] B. Dingfelder and J. A. C. Weideman, Numer. Algor. **68**, 167 (2014).
[71] See Supplemental Material at http://link.aps.org/supplemental/10.1103/PhysRevE.94.033301 for the atomic trajectories recorded during the GFMD and MD simulations.
[72] P. Giannozzi, S. deGironcoli, P. Pavone, and S. Baroni, Phys. Rev. B **43**, 7231 (1991).
[73] P. Giannozzi *et al.*, J. Phys. Condens. Matter **21**, 395502 (2009).
[74] P. T. Harker and J. S. Pang, Lect. Appl. Math. **26**, 265 (1990).
[75] F. H. Yi and L. J. Xian, Commun. Theor. Phys. **36**, 541 (2001).
[76] J. M. Ziman, *Principles of the Theory of Solids*, 2nd ed. (Cambridge University Press, New York, 1971).
[77] M. Berkowitz, J. D. Morgan, and J. A. McCammon, J. Chem. Phys. **78**, 3256 (1983).
[78] O. M. Braun, M. Peyrard, V. Bortolani, A. Franchini, and A. Vanossi, Phys. Rev. E **72**, 056116 (2005).
[79] J. P. Perdew, K. Burke, and M. Ernzerhof, Phys. Rev. Lett. **77**, 3865 (1996).
[80] D. Vanderbilt, Phys. Rev. B **41**, 7892(R) (1990).
[81] N. S. Gillis, N. R. Werthamer, and T. R. Koehler, Phys. Rev. **165**, 951 (1968).
[82] M. Hirano, Surf. Sci. Rep. **60**, 159 (2006).